

# Draft – Effect of Atmospheric Heatwaves on Reflectance and Pigment Composition of Intertidal *Nanozostera noltei* – Draft

Simon Oiry<sup>a,\*</sup>, Bede Ffinian Rowe Davies<sup>a</sup>, Philippe Rosa<sup>a</sup>, Augustin Debly<sup>a</sup>, Anne-Laure Barillé<sup>b</sup>, Nicolas Harrin<sup>b</sup>, Pierre Gernez<sup>a</sup>, Laurent Barillé<sup>a</sup>

<sup>a</sup>*Institut des Substances et Organismes de la Mer, ISOMer, Nantes Université, UR 2160, F-44000 Nantes, France,*

<sup>b</sup>*Bio-littoral, Immeuble Le Nevada, 2 Rue du Château de l'Eraudière, 44300 Nantes, France,*

---

## Abstract

To be written

**Keywords:** Remote Sensing, Pigment Composition, Seagrass, Coastal Ecosystems, Heatwaves

---

## 1. Introduction

Intertidal seagrasses play a crucial role in the ecosystem by providing habitats and feeding grounds for various marine species, supporting rich marine biodiversity, and contributing significantly to primary production and carbon sequestration [1, 2]. These seagrasses are essential in maintaining the health of coastal ecosystems by stabilizing sediments, filtering water, and serving as indicators of environmental changes due to their sensitivity to water quality variations [3]. The interactions between seagrass meadows and their associated herbivores further enhance the delivery of ecosystem services, including coastal protection and fisheries support [4, 5, 6]. Understanding and preserving these ecosystems are vital for maintaining the biodiversity and productivity of coastal regions [7, 8].

Despite their crucial role in marine ecosystems, intertidal seagrasses face numerous threats that compromise their health and functionality. Coastal development and human activities are primary threats. These activities not only reduce the available habitat for seagrasses but also increase water turbidity, which limits light penetration and hampers photosynthesis [9]. Seagrasses are also

---

\*Corresponding author  
Email address: [oiry\\_simon@gmail.com](mailto:oiry_simon@gmail.com) (Simon Oiry)

threatened by nutrient enrichment from agricultural and urban runoff, which can lead to eutrophication. This condition promotes the overgrowth of algal blooms that compete with seagrasses for light and nutrients, further stressing these important plants [10] (Oiry et al. 2024). Pollution from industrial and agricultural fields sources introduces harmful chemicals and heavy metals into coastal waters, posing toxic risks to seagrass health. These pollutants can affect the physiological processes of seagrasses, reducing their growth and survival rates [11]. Additionally, invasive species can out compete native seagrasses for resources, altering community structure and function [12].

Heatwaves, exacerbated by climate change, pose a growing threat to seagrasses. Marine Heatwaves (MHW), defined by [13] as prolonged discrete anomalously warm water events, and Atmospheric Heatwaves (AHW), defined by [14] as periods of at least three consecutive days with temperatures exceeding the 90th percentile, cause severe physiological stress on seagrasses [15, 16]. At the interface between the land and oceans, intertidal seagrasses are exposed to both MHW and AHW. Heatwaves have profound impacts on seagrasses, with their effects varying based on species and geographic location. For instance, the seagrass *Zostera marina* exhibits high susceptibility to elevated sea surface temperatures during winter and spring, leading to advanced flowering, high mortality rates, and reduced biomass [15]. Similarly, *Cymodocea nodosa* shows increased photosynthetic activity during heatwaves but suffers negative effects on photosynthetic performance and leaf biomass during recovery [16]. Additionally, different populations of *Zostera marina* along the European thermal gradient exhibit varied photophysiological responses during the recovery phase of heatwaves, indicating differential adaptation capabilities among populations [17]. These events intensify other stressors, such as overgrazing and seed burial, compromising sexual recruitment [18].

Bleaching and darkening events of seagrass beds have been observed following episodes of intense heat along the Brittany coast of France (Pers. obs.) then affecting leaf color, which are expected to alter leaf reflectance. Remote sensing is increasingly being utilized to monitor marine ecosystems, including seagrass meadows. By using spectral indices, such as the Normalized Difference Vegetation Index (NDVI) and the Soil-Adjusted Vegetation Index (SAVI), or by analyzing specific spectral patterns, remote sensing can effectively quantify vegetation health over time [19, 20, 21, 22]. Through the Water Framework Directive and the Marine Strategy Framework Directive, Europe is promoting remote sensing techniques for habitat mapping, as these methods enable the monitoring of extensive areas over time [23]. This study will experimentally test the hypothesis that warm events modify the pigment composition and reflectance of seagrass, linking these changes with satellite remote sensing.

## 2. Material & Methods

### 2.1. Observation of seagrass leaves darkening.

#### 2.1.1. Field Observation

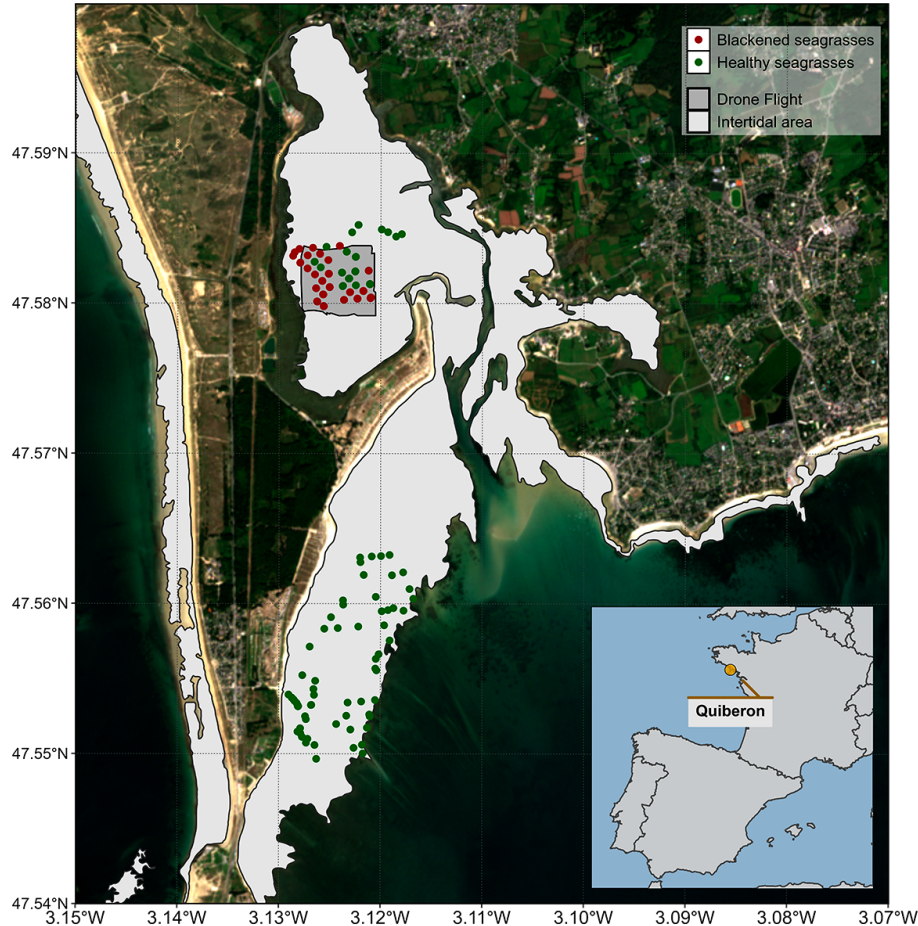


Figure 1: Location of the fieldtrip campaign that occurred in the 10th of September 2021. The light grey polygons indicates the intertidal zone (Zone between High tide and low tide, that is totally emerged at low tide) and the dark grey polygon indicate the extent of the drone flight. Green dots indicate location of quadrat picture over healthy seagrasses while red dots indicate location of quadrat took over darkened seagrasses.

A fieldtrip, aiming to map a seagrass meadow near Quiberon (France :  $46^{\circ}57'32.0''\text{N}$ ,  $2^{\circ}10'37.0''\text{W}$ ), occurred in the 10th of September 2021 Figure 1. During this fieldtrip, darkening of seagrasses have been observed, resulting in the darkening of seagrass leaves over large area of the meadow Figure 2. During this field trip, drone flights were conducted over two areas of the seagrass meadow using a DJI Matrice 200 equipped with a Sequoia Multispectral camera.

The Sequoia captures four spectral bands: Green ( $550 \pm 40$  nm), Red ( $660 \pm 40$  nm), RedEdge ( $735 \pm 10$  nm), and Near Infrared ( $790 \pm 40$  nm). A total of 285 Ground Control Points (GCPs) were collected in the form of georeferenced quadrat images across the meadow. These images allow for visual assessment of vegetation type, density, and health status. The images were then divided into two categories: Healthy seagrasses and darkened seagrasses, based on a visual estimation of the leaf condition Figure 1.

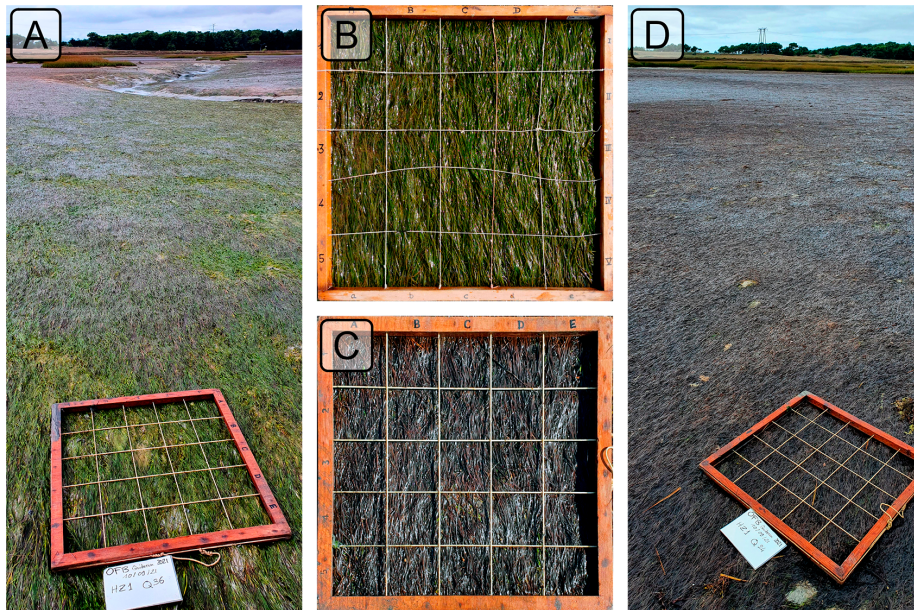


Figure 2: Illustrations of the two health conditions of seagrasses observed in the field. A: Global view of a healthy green meadow; B: Quadrat images of healthy seagrasses; C: Quadrat images of darkened seagrasses; D: Global view of an unhealthy darkened meadow. All images were taken on September 10th, 2021, in Quiberon.

### 2.1.2. Satellite Observation

Add S2 paragraph.

### 2.1.3. Temperature Data and identification of heatwaves

#### 2.1.3.1. Air temperature.

Since January 1, 2024, Meteo France weather data has been freely and openly accessible. Hourly air temperature data ( $^{\circ}\text{C}$ ) for the French Atlantic and Channel coasts was retrieved using a [custom script](#) as no API was available at the time of this study. Weather stations located within 10 kilometers of the coastline were considered, but only those with at least 30 years of data were included to ensure reliable climatological reconstruction. Of the 156 weather stations within 10 kilometers of the coast, only 36 had sufficient data for climatology reconstruc-

tion. The hourly data was then aggregated into daily mean temperatures for each station.

Heatwave detection was performed using the HeatwaveR package in R [24]. This package utilizes the methodology proposed by [13] to detect heatwave events. The climatology for the year was computed using the temperature time series. An event was considered a heatwave each time the temperature exceeded the 90th percentile of the climatology for three consecutive days. The severity of each event has been assessed using the methodology proposed by [25]. Following the methodology of [26], coldspell events corresponding to temperature bellow the percentile 10th of the climatology during 3 consecutives days have also been measured.

Concerning heatwaves event near Quiberon, this methodology has been apply solely on the nearest weather station of our study site (Lorient-Lann Bihoue, 47°45'46"N 3°26'11"W , more than 395000 observation since the 1st of February 1952).

#### 2.1.3.2. Water temperature.

Sea Surface Temperature (SST) data were downloaded from the Copernicus CMEMS platform [27] for the French coast, covering the period from 1982 to 2022. Only pixels within an area of 2700 km<sup>2</sup> around Quiberon, Brittany, France (47°29'03" N, 3°07'09" W) were extracted and analyzed. This area was large enough to minimize missing values caused by cloud cover, yet small enough to avoid being influenced by the stability of offshore SST. After the masking step, a daily average of the remaining pixels was calculated, resulting in a daily mean SST value for the entire time series. Using this daily average since 1982, the SST climatology was computed with the HeatwaveR package in R [24]. The same methodology used to detect air temperature events was applied to identify SST events.

## 2.2. Laboratory experiment

### 2.2.1. Sampling and acclimation of seagrasses

Seagrass was sampled from a *Nanozostera noltei* (dwarf eelgrass, syn. *Zostera noltei*) meadow on Noirmoutier Island, France (46°57'32.0"N, 2°10'37.0"W) at low tide in June 2024. A home-made inox sampling box was used to sample seagrass from an area of 30 cm by 15 cm and 5 cm deep, maintaining the sediment structure and avoiding damage to the rhizomes and the leafs of the seagrass (Figure 3 A). This sampling box allowed to limitate sampling variability between replicates. The seagrass, along with sediment, meiofauna, and macrofauna, was placed in plastic trays. To avoid hydric stress during transportation, seawater was added to each tray. Simultaneously, seawater was sampled from a nearby site and transported to the lab, where it was filtered using a 0.22 µm nitrocellulose filter to remove all suspended particulate matter. This seawater was used in the acclimation tank and the intertidal chambers. The seagrasses were acclimated at high tide for one weeks with a water temperature of 17°C, matching

the temperature at the time of sampling, and with light of  $150 \text{ pmol.s}^{-1}\text{m}^{-2}$  of PAR photons [22]. A wave generator was used in the tank to circulate and reoxygenate the water.

### 2.2.2. Experimental design



Figure 3: Illustrations of the various steps of the experiment. A: Field sampling of seagrass using a homemade sampling box; B: Intertidal chambers used during the experiment; C: Seagrass sample inside a chamber during the experiment at high tide; D: Photo of the treatment sample at the start of the experiment; E: Photo of the treatment sample at the end of the experiment.

Two intertidal chambers from [ElectricBlue](#) were used to simulate tidal cycles and control water temperature during high tide and air temperature during low tide (Figure 3 B,C). One chamber served as the control, while the other was used for the experimental treatment. The control chamber was maintained at temperatures representative of the typical seasonal conditions: water temperatures between  $18^\circ\text{C}$  and  $19^\circ\text{C}$  and air temperatures between  $18^\circ\text{C}$  and  $23^\circ\text{C}$ ,

following circadian temperature variability (Figure 4 left). For the experimental treatment, the air temperature was set to mimic an atmospheric heatwave that occurred over the seagrass meadow of Porth Saint-Guénél, Plouharnel, France ( $47^{\circ}35'40.0''\text{N}$ ,  $3^{\circ}07'30.0''\text{W}$ ) from August 26, 2021, to September 6, 2021. On the first day of the experiment, air temperatures in the experimental chamber were set to range from  $23^{\circ}\text{C}$  at night to  $35^{\circ}\text{C}$  during the day, with a daily increase of  $1^{\circ}\text{C}$ . The water temperature in the experimental chamber was similarly adjusted to reflect the heatwave conditions, starting from the normal seasonal range ( $18^{\circ}\text{C}$ ) and gradually increasing to simulate the rising temperatures experienced during the heatwave ( $+0.5^{\circ}\text{C}$  daily). This setup aimed to replicate the thermal stress experienced by the seagrass meadow during the actual heatwave event (Figure 4 right).

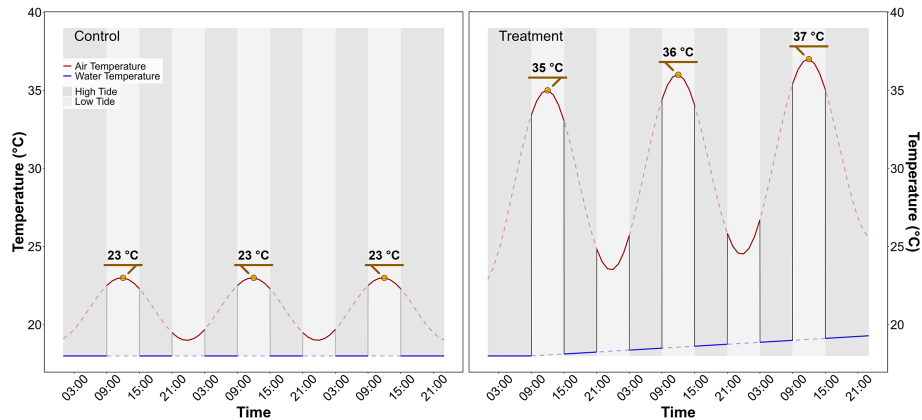


Figure 4: Temperature profiles of both the control (left) and the treatment (right) followed during the heatwave experiment. The red line indicates air temperature, whereas the blue line indicates water temperature. Due to the tidal cycle followed during the experiment, the seagrasses only experience temperatures represented by solid lines.

### 2.2.3. Bio-optical measurements over seagrass leaves

#### 2.2.3.1. Hyperspectral measurements.

Throughout the experiment, hyperspectral signatures of both the control and treatment seagrasses were taken using an ASD HandHeld 2 equipped with a fiber optic, allowing measurements to be taken directly inside the chamber without opening it. Automatic spectra acquisition has been done using the [RS3 software](#) developed by the instrument manufacturer. An average of five reflectance spectrum ( $R(\lambda)$ ), each with an integration time of 544 ms, was taken every minute. Every 10 minutes, the fiber optic was switched from one benthic chamber to the other, in order to measure reflectance in both treatment and control. Because light conditions were controlled inside of the chambers, reflectance calibration of the instrument was performed only each morning at the very first moment of low tide using a Spectralon white reference with 99% Lambertian

reflectivity.

The second derivative of  $R$  was calculated to retrieve absorption features and compare their variability over time. Two radiometric indices were also monitored throughout the experiment :

- The Normalized Difference Vegetation Index (NDVI, [28]), as a proxy of the concentration of chlorophyll-a (Equation 1)

$$NDVI = \frac{R(840) - R(668)}{R(840) + R(668)} \quad (1)$$

where  $R(840)$  and  $R(668)$  are the reflectance at 840 nm and 668 nm respectively.

- The Green Leaf Index (GLI, [29]), as a measurement of the greenness of seagrass leafs (Equation 2)

$$GLI = \frac{[R(550) - R(668)] + [R(550) - R(450)]}{(2 \times R(550)) + R(668) + R(450)} \quad (2)$$

where  $R(550)$  and  $R(450)$  are the reflectance in green at 550 nm and in the blue at 450 nm, respectively.

- The Mid-Infrared Water Absorption Index (MIWAI), proposed here and designed to measure water absorption at 970 nm (**REF**), estimates the difference between the reflectance at 970 nm and a linear interpolation of the reflectance values at 950 and 990 nm. This interpolation represents the expected reflectance value in the absence of water.

$$MIWAI = 0.5 \times [R(990) + R(950)] - R(970) \quad (3)$$

where  $R(990)$ ,  $R(970)$  and  $R(950)$  are the reflectance in the infrared at 990, 970 and 950 nm, respectively.

#### *2.2.3.2. Multispectral imagery measurement.*

Parallel to hyperspectral measurements, multispectral images were taken at the beginning and end of each diurnal low tide (09:00 am and 03:00 pm). A Micasense RedEdge-MX Dual multispectral camera, originally designed to be mounted on a drone, was modified for use without a drone. A 3D-printed mount was designed to attach the camera to the intertidal chamber and ensure that each picture was captured under the same conditions. At each time step (09:00 am and 03:00 pm), a first picture of the Spectralon was taken to allow for image correction in reflectance, followed by a second picture

of the target. [DISCOV](#), a Neural Network classification model previously developed to map intertidal vegetation using drone imagery, has been applied to each image taken inside the intertidal chambers. To understand the behavior of the model on seagrasses affected by heatwaves, classification images from before and after the heatwave have been compared.

#### 2.2.3.3. *Pigment concentration measurements.*

At the beginning and the end of each diurnal low tide (09:00 am and 03:00 pm) leaves samples have been took in both the test and the control. leaves sampled have been stored under -80°C waiting for analysis. Pigment composition and biomass were analyzed using high-performance liquid chromatography (HPLC). The HPLC system (Alliance HPLC 248 System, Waters) was equipped with a reverse-phase C-18 separating column (SunFire C-18 Column, 100Å, 3.5 µm, 2.1 mm x 50 mm, Waters), preceded by a precolumn (VanGuard 3.9 mm x 5 mm, Waters). The system also included a photodiode array detector (2998 PDA) and a fluorimeter (Ex: 425 nm, Em: 655 nm; RF-20A, SHIMADZU).

**Au secours Philippe !!!**

### 3. Results

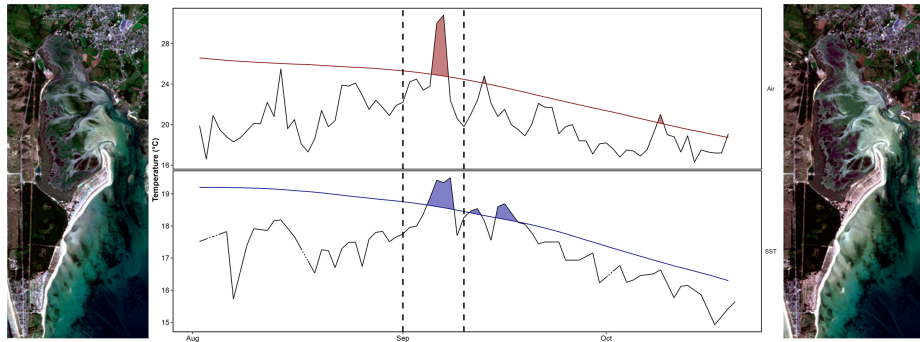


Figure 5: Visual inspection of the meadow before (left) and after (right) of both marine heatwave and atmospheric heatwave (center). In the center plot, colored lines show 90th percentile of SST (blue) and air temperature (red), while colored polygons represent Marine heatwave (blue) and atmospheric heatwave (red). Darklines represent air temperature (top) and SST (bottom).

### Bibliography

- [1] R. K. Unsworth, L. C. Cullen-Unsworth, B. L. Jones, R. J. Lilley, The planetary role of seagrass conservation, *Science* 377 (6606) (2022) 609–613.
- [2] A. I. Sousa, J. F. da Silva, A. Azevedo, A. I. Lillebø, Blue carbon stock in *zostera noltei* meadows at ria de aveiro coastal lagoon (portugal) over a decade, *Scientific reports* 9 (1) (2019) 14387.

- [3] M. L. Zoffoli, P. Gernez, L. Godet, S. Peters, S. Oiry, L. Barillé, Decadal increase in the ecological status of a north-atlantic intertidal seagrass meadow observed with multi-mission satellite time-series, *Ecological Indicators* 130 (2021) 108033.
- [4] E. Jankowska, L. N. Michel, G. Lepoint, M. Włodarska-Kowalcuk, Stabilizing effects of seagrass meadows on coastal water benthic food webs, *Journal of Experimental Marine Biology and Ecology* 510 (2019) 54–63.
- [5] M. L. Zoffoli, P. Gernez, S. Oiry, L. Godet, S. Dalloyau, B. F. R. Davies, L. Barillé, Remote sensing in seagrass ecology: coupled dynamics between migratory herbivorous birds and intertidal meadows observed by satellite during four decades, *Remote Sensing in Ecology and Conservation* 9 (3) (2023) 420–433.
- [6] R. C. Gardner, C. Finlayson, Global wetland outlook: state of the world's wetlands and their services to people, in: Ramsar convention secretariat, 2018, pp. 2020–5.
- [7] A. L. Scott, P. H. York, C. Duncan, P. I. Macreadie, R. M. Connolly, M. T. Ellis, J. C. Jarvis, K. I. Jinks, H. Marsh, M. A. Rasheed, The role of herbivory in structuring tropical seagrass ecosystem service delivery, *Frontiers in Plant Science* 9 (2018) 127.
- [8] C. Ramesh, R. Mohanraju, Seagrass ecosystems of andaman and nicobar islands: Status and future perspective., *Environmental & Earth Sciences Research Journal* 7 (4) (2020).
- [9] M. Waycott, C. M. Duarte, T. J. Carruthers, R. J. Orth, W. C. Dennison, S. Olyarnik, A. Calladine, J. W. Fourqurean, K. L. Heck Jr, A. R. Hughes, et al., Accelerating loss of seagrasses across the globe threatens coastal ecosystems, *Proceedings of the national academy of sciences* 106 (30) (2009) 12377–12381.
- [10] E. Thomsen, L. S. Herbeck, I. G. Viana, T. C. Jennerjahn, Meadow trophic status regulates the nitrogen filter function of tropical seagrasses in seasonally eutrophic coastal waters, *Limnology and Oceanography* 68 (8) (2023) 1906–1919.
- [11] K. Sevgi, S. Leblebici, Bitkilerde ağır metal stresine verilen fizyolojik ve moleküler yanıtlar, *Journal of Anatolian Environmental and Animal Sciences* 7 (4) (2022) 528–536.
- [12] T. S. Simpson, T. Wernberg, J. I. McDonald, Distribution and localised effects of the invasive ascidian *didemnum perlucidum* (monniot 1983) in an urban estuary, *PLoS One* 11 (5) (2016) e0154201.
- [13] A. J. Hobday, L. V. Alexander, S. E. Perkins, D. A. Smale, S. C. Straub, E. C. Oliver, J. A. Benthuyzen, M. T. Burrows, M. G. Donat, M. Feng,

et al., A hierarchical approach to defining marine heatwaves, *Progress in oceanography* 141 (2016) 227–238.

- [14] S. E. Perkins, L. V. Alexander, On the measurement of heat waves, *Journal of climate* 26 (13) (2013) 4500–4517.
- [15] Y. Sawall, M. Ito, C. Pansch, Chronically elevated sea surface temperatures revealed high susceptibility of the eelgrass *zostera marina* to winter and spring warming, *Limnology and Oceanography* 66 (12) (2021) 4112–4124.
- [16] A. Deguette, I. Barrote, J. Silva, Physiological and morphological effects of a marine heatwave on the seagrass *cymodocea nodosa*, *Scientific Reports* 12 (1) (2022) 7950.
- [17] G. Winters, P. Nelle, B. Fricke, G. Rauch, T. B. Reusch, Effects of a simulated heat wave on photophysiology and gene expression of high-and low-latitude populations of *zostera marina*, *Marine Ecology Progress Series* 435 (2011) 83–95.
- [18] L. Guerrero-Meseguer, A. Marín, C. Sanz-Lázaro, Heat wave intensity can vary the cumulative effects of multiple environmental stressors on *posidonia oceanica* seedlings, *Marine Environmental Research* 159 (2020) 105001.
- [19] A. R. Huete, Vegetation indices, remote sensing and forest monitoring, *Geography Compass* 6 (9) (2012) 513–532.
- [20] S. Kloos, Y. Yuan, M. Castelli, A. Menzel, Agricultural drought detection with modis based vegetation health indices in southeast germany, *Remote Sensing* 13 (19) (2021) 3907.
- [21] I. Cârlan, B.-A. Mihai, C. Nistor, A. Große-Stoltenberg, Identifying urban vegetation stress factors based on open access remote sensing imagery and field observations, *Ecological Informatics* 55 (2020) 101032.
- [22] M. Akbar, P. Arisanto, B. Sukirno, P. Merdeka, M. Priadhi, S. Zallesa, Mangrove vegetation health index analysis by implementing ndvi (normalized difference vegetation index) classification method on sentinel-2 image data case study: Segara anakan, kabupaten cilacap, in: *IOP Conference Series: Earth and Environmental Science*, Vol. 584, IOP Publishing, 2020, p. 012069.
- [23] E. Papathanasopoulou, S. Simis, K. Alikas, A. Ansper, J. Anttila, A. Barillé, L. Barillé, V. Brando, M. Bresciani, M. Bučas, et al., Satellite-assisted monitoring of water quality to support the implementation of the water framework directive, *EOMORES white paper* (2019).
- [24] R. W. Schlegel, A. J. Smit, heatwaveR: A central algorithm for the detection of heatwaves and cold-spells, *Journal of Open Source Software* 3 (27) (2018) 821. [doi:10.21105/joss.00821](https://doi.org/10.21105/joss.00821).

- [25] A. J. Hobday, E. C. Oliver, A. S. Gupta, J. A. Benthuysen, M. T. Burrows, M. G. Donat, N. J. Holbrook, P. J. Moore, M. S. Thomsen, T. Wernberg, et al., Categorizing and naming marine heatwaves, *Oceanography* 31 (2) (2018) 162–173.
- [26] R. W. Schlegel, E. C. Oliver, T. Wernberg, A. J. Smit, Nearshore and offshore co-occurrence of marine heatwaves and cold-spells, *Progress in Oceanography* 151 (2017) 189–205.
- [27] CMEMS, European north west shelf/iberia biscay irish seas – high resolution odyssea sea surface temperature multi-sensor l3 observations reprocessed, e.u. copernicus marine service information (cmems). marine data store (mds). (accessed on 17-10-2024) (2024). [doi:10.48670/moi-00311](https://doi.org/10.48670/moi-00311).
- [28] J. W. Rouse, R. H. Haas, J. A. Schell, D. W. Deering, et al., Monitoring vegetation systems in the great plains with erts, *NASA Spec. Publ* 351 (1) (1974) 309.
- [29] M. Louhaichi, M. M. Borman, D. E. Johnson, Spatially located platform and aerial photography for documentation of grazing impacts on wheat, *Geocarto International* 16 (1) (2001) 65–70.